Journal of Electroceramics 2:2, 95–104, 1998

Defect-Property Correlations in Garnet Crystals. *VII: The Electrical Conductivity and Defect Structure of Yttrium Aluminum and Yttrium Iron Garnet Solid Solutions

S.R. ROTMAN

Department of Electrical and Computer Engineering, Ben-Gurion University of the Negev, P.O. Box 653, 84105 Beer-Sheva, Israel

H.L. TULLER

Crystal Physics and Electroceramics Laboratory, Center for Materials Science and Engineering, Massachusetts Institute of Technology, Cambridge, MA 02139

Submitted November 18, 1997; Revised April 10, 1998; Accepted April 10, 1998

Abstract. The conduction mechanisms in yttrium aluminum and yttrium iron garnet solid solutions have been studied as a function of temperature, iron concentration and partial pressure of oxygen. At low concentrations of iron, ac conductivity and ionic transference measurements show the solid solution to be a mixed ionic-electronic conductor with an ionic mobility characterized by an activation energy of 2.6–2.8 eV and a *p*-type electronic conductivity with activation energy of 3.0–3.3 eV. High concentrations of iron cause a dramatic increase in the electrical conductivity connected with the formation of an Fe impurity band found to lie 1.9 eV below the conduction band. Transport through this band is via an activated hopping process with an activation energy of 0.7 eV for 6 fraction percent Fe. A defect model is presented which is consistent with our experimental observations including the conductivity maxima obtained at high Po_2's for high Fe levels.

Keywords: electrical conductivity, defects, garnets, YAG, small polaron

1. Introduction

YAG (yttrium aluminum garnet) is of interest as a host for rare-earth and transition-metal ions in laser [1–3] and phosphorescent sources [4]. Because the emission efficiency of neodymium-doped YAG (Nd : YAG) lasers [5] and cerium-doped YAG (Ce : YAG) [6] phosphors can be strongly influenced by defects and inadvertent dopants, it becomes important to develop models which enable optimization of the fabrication process.

In previous papers on this subject [7–12] we examined the electrical and optical properties of cerium (Ce : YAG), nickel (Ni : YAG), and calcium-doped (Ca : YAG) yttrium aluminum garnet. Based on these results, the oxygen vacancy was found to play a key role in influencing the luminescence and mass transport properties of YAG. In particular [8], Ce : YAG was shown to be a mixed ionic-electronic conductor with an activation energy for ionic conduction of 2.3 V. The oxygen vacancy concentration was fixed by the background acceptor dopant density introduced into the crystal during growth. Of special interest was the case of nickel which led to a Po_2-dependent ionic conductivity [10] as a consequence of its variable valence (i.e., Ni^{2+}, Ni^{3+}). The influence of these defects on optical absorption and photoluminescence was also examined [9,11].

Recently, we studied the luminescent properties of YIG-YAG ($Y_3Fe_5O_{12}$- $Y_3Al_5O_{12}$) solid solutions [13] in which we found energy transfer between oxygen vacancy optical emission and iron absorption bands. In this paper, we examine the electrical properties of

* The first six documents in this series are listed as items 8 through 13 in the reference section to this article.

aluminum-rich yttrium aluminum and yttrium iron garnet solid solutions ($Y_3Al_{5-x}Fe_xO_{12}$) as a function of iron concentration, temperature and partial pressure of oxygen. These data assist us in identifying the nature of the primary defects and the valence states of the iron and thus enable us to propose a defect model consistent with our measurements. By correlating the optical and electrical properties, a qualitative and quantitative picture of the defect structure of the solid solution is obtained.

Three previous conductivity studies in YAG, besides our own, have been reported. Bates and Garnier [14] presented electrical conductivity data as a function of temperature under oxidizing conditions for nominally undoped YAG. No attempt was made to model these results. Neiman, Tkachenko, and Zhukovskii [15] performed limited ionic transference and conductivity measurements on $Y_3Al_5O_{12}$, $Y_3Fe_5O_{12}$ and $Y_3Ga_5O_{12}$ and concluded that YAG was a mixed ionic-electronic conductor under oxidizing conditions. However, the effects of impurities on the crystal's defect structure were not considered; all defects were considered to be intrinsic—a highly unlikely situation. Finally, Schuh et al. [16] reported that polycrystalline calcium-doped YAG is a mixed ionic-electronic conductor with an ionic activation energy of about 2 eV. However, due to the presence of an alumina second phase, they proposed the primary defects to be aluminum vacancies. We have noted, however, that Schuh et al.'s results are more consistent with the oxygen vacancy defect model [12].

2. Experimental Techniques

Single crystals of $Y_3Al_{5-x}Fe_xO_{12}$ were grown via the floating zone crystal growth method from polycrystalline feed rods, utilizing a 1500 W CO_2 laser as the heat source [17–19]. A detailed description of the growth procedure and specimen analysis has been previously reported [13]. The samples in [13] were labeled by the iron-percentage in the feed rod, i.e., 0%, 0.1%, 1%, and 10%; the actual concentrations in the crystal were found to be approximately one-fifth of that in the melt (see Table 1). For consistency, we will maintain the nomenclature used in [13] in this paper. In addition, a fifth sample was made with 10% Fe in the feed rod; however, only one pass with the laser was performed during crystallization resulting in 6% Fe in the crystal. We refer to this most heavily doped crystal as 10%Fe* : YAG. Note, in this study we do not evaluate the specimen Fe = 10% (2% in crystal).

Table 1. Iron concentrations prior and subsequent to growth of single crystals

Prior to Growth	Subsequent to Growth
Fe = 0%	Fe < 0.1%
Fe = 0.1%	Fe < 0.1%
Fe = 1%	Fe = 0.2%
Fe = 10%	Fe = 2.0%
Fe = 10%*	Fe = 6.0%

AC complex impedance measurements were performed using an in-house designed cross correlator, which measures the real and imaginary impedance at each frequency, thus allowing electrode and bulk effects to be analyzed separately. The conductivities were measured over a wide range of temperatures (in some cases 500°C to 1320°C) while different Po_2's were maintained by flowing mixtures of argon/oxygen or CO_2/CO gas combinations. In addition, transference measurements were performed using an apparatus previously described in detail in [8]. A zirconia concentration cell, placed in series with the sample chamber, was used to measure the Po_2 of each of the gas mixtures used in these studies.

3. Theory

3.1. Fixed Aliovalent Doped Oxide

To understand the defect structure of $Y_3Al_{5-x}Fe_xO_{12}$, we must first consider the model we previously derived for iron-free YAG. We will assume an oxygen vacancy model, based on work performed by Larsen and Metselaar on YIG [20–24] and ourselves on Ce : YAG and Ni : YAG [8–10].

Assuming the oxygen vacancy model, several quasi-chemical reactions need be considered. First, we have the intrinsic generation and recombination of electrons and holes across the band gap. Using Kröger–Vink notation [25] this can be expressed as

$$O \rightarrow e' + h \tag{1a}$$

with the mass-action relation yielding an *np* product of the form

$$np = K_i(T) = K_i^O \exp(-E_g/kT) \tag{1b}$$

where E_g is the thermal energy gap of the crystal.

Second, we consider the production of doubly ionized oxygen vacancies, $V_0^{\bullet\bullet}$, by the removal of oxygen from the crystal into the gas phase.

$$O_o \leftrightarrow V_0^{\bullet\bullet} + 2e' + \frac{1}{2}O_2 \tag{2a}$$

The corresponding mass-action relation is given by

$$\begin{aligned} n^2[V_0^{\bullet\bullet}] &= K_1(T)Po_2^{-1/2} \\ &= K_1^0 \exp(-E_1/kT)Po_2^{-1/2} \end{aligned} \tag{2b}$$

in which Po_2 is the partial pressure of oxygen and E_1 the energy characterizing the redox process.

Finally, we consider the requirement of charge neutrality. This is described by the relation

$$n + [A'] = p + 2[V_0^{\bullet\bullet}] \tag{3}$$

in which we have assumed impurity domination by singly ionized acceptors A′. As before, the predominant lattice defect is assumed to be a doubly-ionized oxygen vacancy. Following conventional practice, we simplify the analysis by examining the solutions for the unknown defect species under conditions for which the neutrality equation can be simplified to only two terms.

Under highly reducing conditions, large concentrations of $V_0^{\bullet\bullet}$ are generated which are balanced by the electrons released into the conduction band and so Eq. (3) is approximated by

$$n = 2[V_0^{\bullet\bullet}] \tag{4a}$$

As the degree of reduction is decreased, a condition of nearly complete compensation is achieved between $V_0^{\bullet\bullet}$ and the acceptor impurity A′. This condition is described by

$$[A'] = 2[V_0^{\bullet\bullet}] \tag{4b}$$

Finally, under oxidizing conditions, Eq. (3) is expected to revert to

$$[A'] = p \tag{4c}$$

Under conditions where the number of vacancies is controlled by inadvertent acceptor dopants (Eq. 4b), the conductivity will be the sum of an electronic *n*-type component (proportional to $Po_2^{-1/4}$), a *p*-type component (proportional to $Po_2^{1/4}$) and a Po_2-independent ionic component (see Eqs. 1b, 2b, and 4b). If this ionic component were to dominate, its activation energy, ignoring association [12] would be that of the ionic mobility. The electron and hole activation energies would be $E_1/2$ and $E_g - E_1/2$, respectively.

3.2. *Variable-Valent Doped Oxide*

Let us consider the effect of a variable-valent dopant on the defect model. Consider iron on an aluminum site; assume that iron can take on either the 3^+ or 4^+ state, depending on the atmosphere and temperature. Ionization of Fe^{3+} to Fe^{4+} is given by

$$Fe_{Al}^x \rightarrow Fe_{Al}^{\bullet} + e' \tag{5}$$

described by the mass-action relation

$$\frac{[Fe_{Al}^{\bullet}]n}{[Fe_{Al}^x]} = K_3(T) = K_3^0 \exp(E_3/kT) \tag{6}$$

Combining Eq. (5) with Eq. (2a) gives

$$2Fe_{Al}^{\bullet} + O_0^x \rightarrow 2Fe_{Al}^x + V_0^{\bullet\bullet} + \frac{1}{2}O_2 \tag{7}$$

which, with the help of Eq. (2b) and Eq. (6), leads to

$$\frac{[V_0^{\bullet\bullet}][Fe_{Al}^x]^2}{[Fe_{Al}^{\bullet}]^2} = Po_2^{1/2}\left(\frac{K_1^0}{(K_3^0)^2}\right)\exp(-(E_1 - 2E_3)/kT) \tag{8}$$

The addition of a variable-valence ion modifies the predictions of the model presented in 3.1 in two important ways. First, the oxygen vacancy concentration can vary as a function of Po_2 due to the variable valence of Fe. A Po_2 dependent ionic conductivity was obtained, as previously noted for Ni : YAG [10]. Second, hopping of holes or electrons can occur between Fe^{3+} and Fe^{4+} ions when the Fe concentration becomes high enough to form an impurity band. Since in the small polaron model the conductivity is proportional to $c(1-c)$ where c is the ratio of Fe^{3+} to the total iron concentration, one expects a maximum in conductivity when $[Fe_{Al}^{\bullet}] \approx [Fe_{Al}^x]$.

4. Results

4.1. *Lightly-Doped Fe : YAG (0%, 0.1%, 1%)*

Figures 1–4 show conductivity isotherms for all the Fe : YAG samples. The 0%, 0.1%, and 1% Fe : YAG samples exhibit qualitatively similar results. A Po_2-

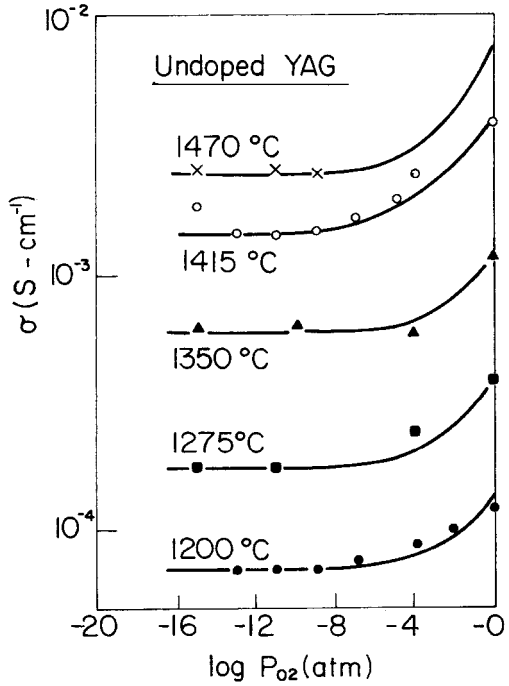

Fig. 1. Conductivity isotherms for 0% Fe : YAG as a function of Po_2.

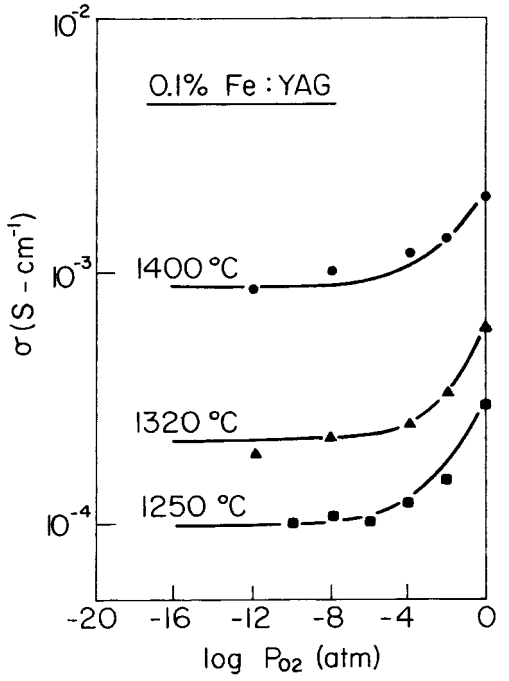

Fig. 2. Conductivity isotherms for 0.1% Fe : YAG as a function of Po_2.

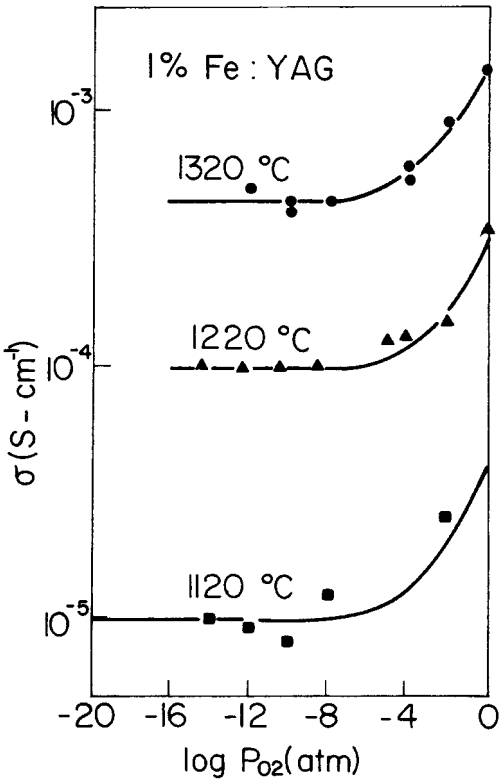

Fig. 3. Conductivity isotherms for 1% Fe : YAG as a function of Po_2.

dependent *p*-type regime is observed under oxidizing conditions, while a Po_2-independent regime dominates for more reducing conditions. We assume that the conductivity σ follows the expression (see model with fixed valent dopant).

$$\sigma_{\text{total}} = \sigma_{\text{ionic}} + \sigma_p^0 Po_2^{1/4} \tag{9}$$

We can extrapolate the Po_2-independent conductivity from the low Po_2 atmospheres to the high Po_2-atmospheres. By subtracting it from the total conductivity, the electronic *p*-type conductivity can be isolated and analyzed. As an example, Fig. 5 shows the separation of the conductivity into ionic and electronic components for the 0.1% sample. The Po_2-dependence of the *p*-type conductivity was fit by a least-squares method to $Po_2^{1/4}$.

The temperature dependence of the ionic and electronic components of the 0%, 0.1%, and 1% Fe : YAG crystals are shown in Figs. 6 and 7, respectively. The activation energies for ionic

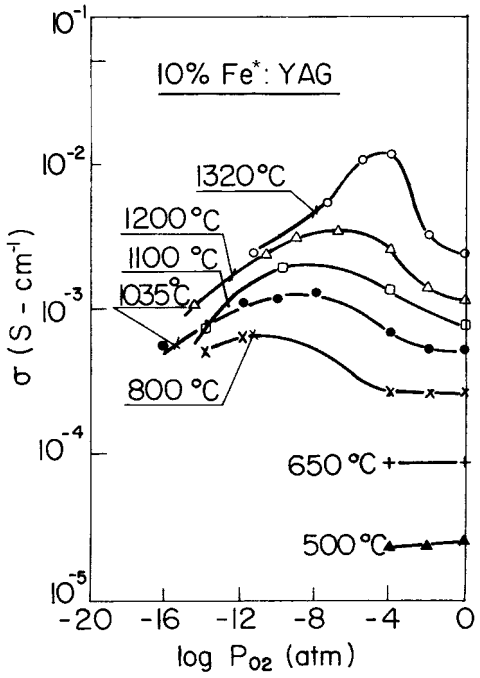

Fig. 4. Conductivity isotherms for 10%* Fe : YAG as a function of Po_2.

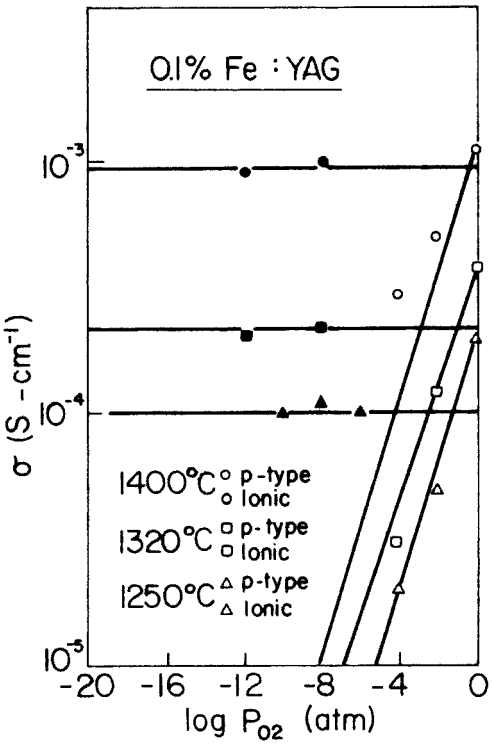

Fig. 5. Ionic and electronic components of the electrical conductivity of 0.1% Fe : YAG. Solid curves represents best fit to data.

conductivity are 2.7, 2.6, and 2.8 eV, while those for the *p*-type conductivity are 3.2, 3.0, and 3.3 eV for the 0%, 0.1%, and 1% samples, respectively. There is surprisingly little dependence of the magnitude of the partial conductivities on Fe content, particularly in the case of the ionic conductivity. We return later to this observation. The sum of the ionic and *p*-type conductivity values, for the respective compositions, are displayed by the solid lines in Figs. 1–3.

4.2. *Heavily-Doped $Y_3Al_{5-x}Fe_xO_{12}$ (10%*)*

The 10% Fe* : YAG crystal shows radically different Po_2 and temperature dependencies (Fig. 4). For the most oxidizing conditions, at reduced temperatures, a Po_2-independent regime is obtained. At elevated temperatures, the conductivity goes through a maximum with decreasing Po_2. The maximum shifts to more oxidizing conditions as the temperature is raised. The Po_2-independent regime at high Po_2 disappears entirely by 1100°C. The activation energy of the Po_2-independent regime at high Po_2 was found to be 0.7 eV (Fig. 8), much lower in

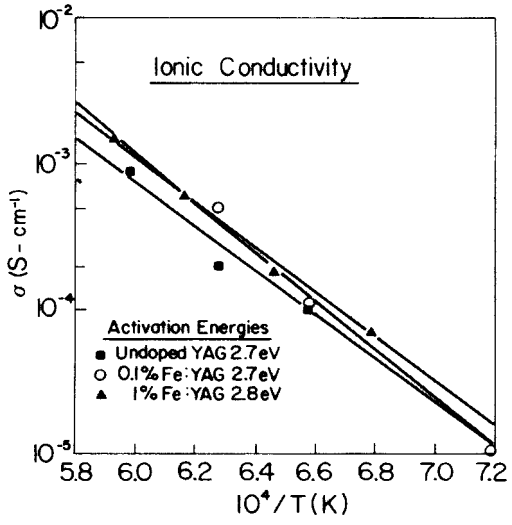

Fig. 6. Temperature dependence of ionic conductivity for Fe : YAG. Solid curves are least square fits to data.

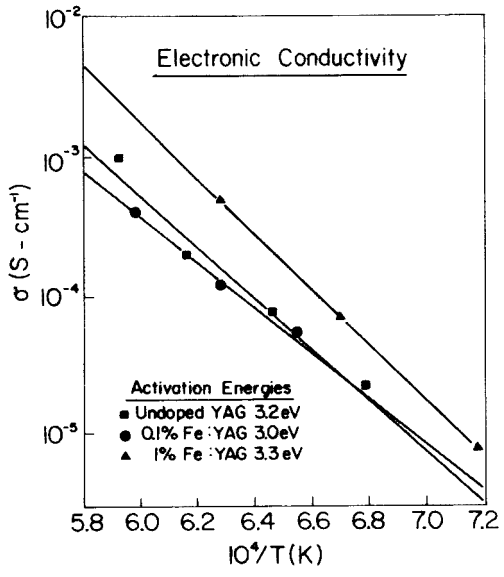

Fig. 7. Temperature dependence of *p*-type conductivity for Fe : YAG. Solid curves are least square fits to data.

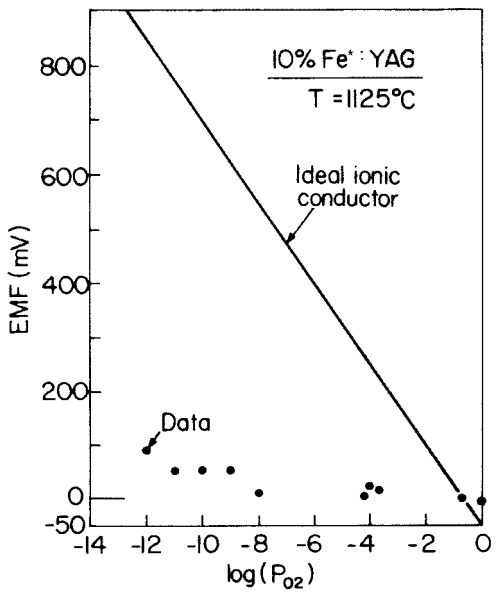

Fig. 9. Ionic transference measurements for 10%* Fe : YAG.

magnitude than the ionic conduction activation energies obtained for Po_2-independent regimes characterized in our other YAG crystals. The ionic transference measurements (Fig. 9) demonstrate that the charge carriers contributing to this regime in 10% Fe* : YAG are predominantly electronic rather than ionic in nature.

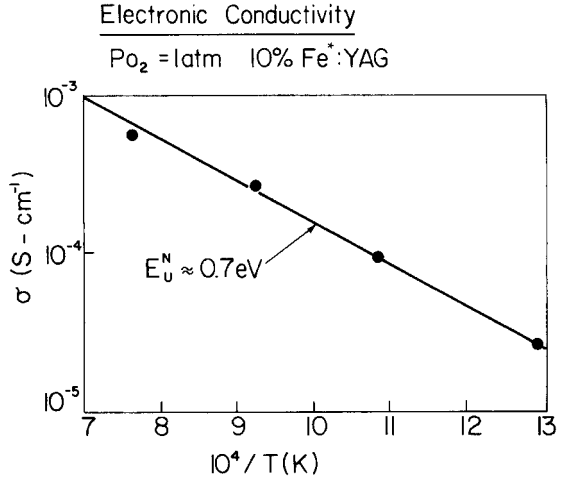

Fig. 8. Temperature dependence of the electronic conductivity of 10%* Fe : YAG for fixed carrier density.

5. Discussion

5.1. Lightly-doped Fe : YAG (0%, 0.1%, and 1%)

The conductivity isotherms for YAG crystals doped with 0%, 0.1%, and 1% iron, respectively, were all qualitatively identical. The iron concentration does not appear to be a significant factor at these levels. The ionic conductivity activation energy of 2.6–2.8 eV is in the range of the measured activation energies for oxygen ion conductivity obtained previously in Ce : YAG [8], Ni : YAG [10], and Ni : Zr : YAG [10].

It is notable, however, that the magnitude of the ionic conductivity is approximately two orders of magnitude greater in these Fe : YAG crystals than the values measured in Ce : YAG [8] and Ni : Zr : YAG [10] crystals previously. This points to a much higher background acceptor level in the Fe : YAG crystal series grown by the laser float zone method. Since the crucible-free float zone method is notable for its ability to minimize contamination during growth, this points to the YAG powder used to prepare the feed rod as the likely source of the contamination.

5.2. Heavily-Doped $Y_3Al_{5-x}Fe_xO_{12}$ (10%)*

For our most heavily doped Fe : YAG crystal, 10% Fe* : YAG (10% in the feed rod, 6% in the crystal), the

conductivity isotherms differed, both qualitatively and quantitatively, from those of the other YAG crystals that we have examined. This represents the only occasion in which we observe a clear conductivity maximum in the isotherms. Transference measurements (Fig. 9) confirm the electronic character of the conductivity. Neutrality in the crystal is no longer determined by doubly-ionized oxygen vacancies compensated by background acceptors Eq. (4b), but rather by the neutrality relation in which

$$[Fe'_{Al}] = [A'] \tag{10}$$

This is consistent with a Po_2-independent electronic-type conduction mechanism under sufficiently oxidizing conductions.

The change of the positive compensating defect from doubly-ionized oxygen vacancies to Fe^{4+} ions, indicates that sufficient Fe has entered the lattice to drive reaction 7 to the left at high Po_2. As increasing levels of iron enter the crystal, the iron defect band also broadens leading to electron hopping between adjacent Fe ions.

As reduction occurs, the number of $V_0^{\bullet\bullet}$ centers should increase while the concentration of Fe^{4+} should decrease, as predicted in Eq. (8). It is well known in the theory of polaronic motion of electronic carriers that electrical conduction is optimized when the ions, between which electron and hole hopping occur are in two states of ionization. Thus, if c is the fraction of Fe^{3+} ions to the total iron level, i.e.,

$$c = [Fe^{3+}]/[Fe_{Tot}] \tag{11}$$

then the conductivity will have a $c(1-c)$ dependence with a maximum at $c = 0.5$. This would explain the observed maxima in the conductivity isotherms [26].

Let us consider the form of the conductivity isotherms that we can expect. The relevant neutrality equation is

$$[Fe'_{Al}] + 2[V_0^{\bullet\bullet}] = [A'] \tag{12}$$

Combining this equation with Eq. (8) and defining

$$K = \frac{[A']}{[Fe_{Tot}]} \tag{13}$$

we obtain

$$\frac{[c-(1-K)]c^2}{(1-c)^2} = \frac{K_1(T)}{(K_3(T))^2}\frac{2}{[Fe_{Tot}]}\mathrm{Po}_2^{-1/2} \tag{14}$$

It is interesting to consider the cases of extreme oxidation and reduction. Under extreme reduction, c approaches 1 ($[Fe^{x}_{Al}] \approx [Fe_{Tot}]$) and the neutrality equation becomes

$$2[V_0^{\bullet\bullet}] = [A'] \tag{15}$$

Equation (14) simplifies to

$$(1-c)^2 \alpha Po_2^{1/2} \tag{16}$$

and the conductivity σ becomes proportional to

$$\sigma \alpha c(1-c)\alpha Po_2^{1/4} \tag{17}$$

Under oxidation

$$[Fe'_{Al}] \approx [A'] \tag{18}$$

or

$$1 - c \approx K \tag{19}$$

This gives a conductivity proportional to

$$\sigma \alpha c(1-c) \approx K(1-K) \tag{20}$$

i.e., the conductivity approaches a constant.

In order to plot Eq. (14), we must approximate K. The maximum value of σ corresponds ideally to $c(1-c) = 0.25$. The ratio of conductivity between the peak and the plateau in the oxidized regime is approximately 2 (see Fig. 4); this yields $c(1-c) \approx 0.12$ and $c \approx 0.15 (1 - c = 0.85)$ in the plateau. Thus, $K \approx 0.85$.

This value of K, as defined in Eq. (13), is rather large, since $[Fe_{Tot}]$ represents the deliberate doping of iron in the crystal while $[A']$ represents inadvertent doping. However, as noted above, the exceptionally high ionic conductivities measured in this series of specimens suggests that $[A']$ approaches the 2000 ppm level.

Equation (14) is plotted in Fig. 10 and compared to the experimental data at $T = 1035°C$. The solid curve was obtained by first noting that at the maximum where $c = 1/2$, the left hand side of the Eq. (14) equals 0.35. Thus one obtains

$$\frac{2}{[Fe_{Tot}]}\frac{K_1(T)}{(K_3(T))^2} \equiv Q(T) = 0.35 Po_2^{1/2}(\max) \tag{21}$$

Substituting $\mathrm{Po}_2(\max) = 10^{-9}$ atm gives Q (1308 K) $= 1.1 \times 10^{-5}$ atm$^{1/2}$. The fit to the data, while good at $\mathrm{Po}_2 > 10^{-12}$ atm, begins to deviate significantly from the predicted $\mathrm{Po}_2^{1/4}$ dependence at low Po_2 (see Eq. 17). The weaker dependence may be

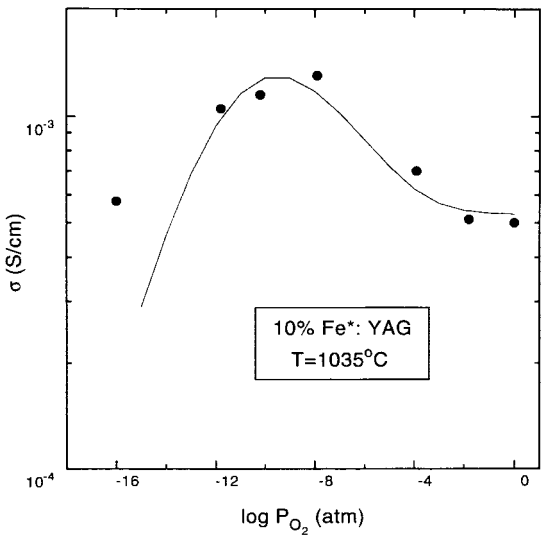

Fig. 10. Comparison of the measured $\log-\sigma$ Po_2 isotherm of 10% Fe : YAG at 1035°C to the theoretical curve predicted by Eq. (14).

related to a Po_2-independent ionic contribution at low Po_2 (see Figs. 1–4) and/or a divergence from the expected $c(1-c)$ behavior.

We must now consider the conductivity as a function of temperature. Even without computing the individual Po_2-dependencies of $V_0^{\bullet\bullet}$, Fe_{Al}^{x} and $Fe_{Al}^{\bullet}$, it is clear from Eq. (8), (see also (Eq. 14)) that any feature of an isotherm, such as the maximum of the conductivity, will occur on each isotherm at a constant value of $Po_2^{-1/2}\exp(-(E_1-2E_3)/kT)$ (assuming that the activation energy of the mobility remains constant). Specifically, it is clear from Eq. (21) that one can obtain the energy term $E_1-2E_3=E_Q$ from a plot of $\log Po_2(\max)$ versus $1/T$. It follows that

$$\log Po_2(\max)=2\log Q+0.91 \tag{22}$$

Figure 11 shows a plot of log $Po_2(\max)$ versus reciprocal temperature from which one derives a value of 8.0 eV for the activation energy. The value of $E_Q=E_1-2E_3$ is thus 4.0 eV as follows from Eq. (22). With the value of $E_1=7.8$ eV derived for Ce : YAG [8], we find the energy to excite an electron from the Fe^{3+} level to the conduction band to be $E_3=1.9$ eV. This puts the Fe^{3+} band at a level 4.2 eV above the oxygen $2p$ band given a band gap of 6.1 eV [8], i.e., above mid gap. This value is in reasonable agreement with the reported value for the band gap of yttrium iron garnet (YIG) of 3 eV [23].

With the above data one obtains an expression for Q, given by

$$Q=2.75\times10^{10}\exp(-4\text{ eV}/kT)\text{atm}^{1/2} \tag{23}$$

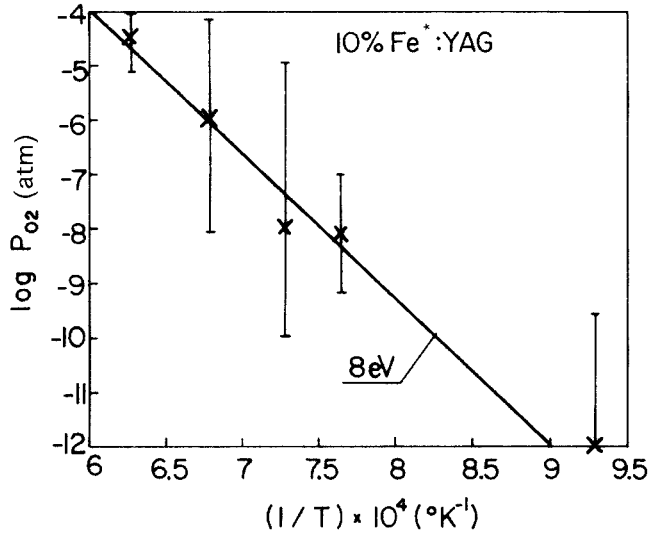

Fig. 11. Temperature dependence of the partial pressure of oxygen for which the maximum conductivity of each conductivity isotherm of 10%* Fe : YAG occurs.

It follows from Eq. (21) and (23) that

$$\frac{K_1^0}{(K_3^0)^2} = \frac{Q_0[Fe_{Tot}]}{2} = 1.38 \times 10^{10}\ \text{atm}^{1/2}[Fe_{tot}] \quad (24)$$

with

$$\begin{aligned}[Fe_{tot}] &= 6\ \text{cation}\ \% \\ &= 0.06 \times 2.3 \times 10^{22}\ \text{Al/cm}^3 \\ &= 1.39 \times 10^{21}\ \text{cm}^{-3}\end{aligned}$$

gives

$$\frac{K_1^0(T)}{(K_3^0(T))^2} = 1.92 \times 10^{31}\,\frac{\text{atm}^{1/2}}{\text{cm}^3} \quad (25)$$

It is readily shown [27] that $K_3^0(T)$ corresponds to the conduction band effective density of states N_c given by

$$\begin{aligned}N_c &= 2.5 \times 10^{19}\ \text{cm}^{-3}(m_n/m_0)^{3/2}\left(\frac{T}{300K}\right)^{3/2} \\ &= 2.3 \times 10^{20}\ \text{cm}^{-3}(T = 1308K)\end{aligned} \quad (26)$$

assuming $m_n = m_o$. It therefore follows from Eq. (25) that

$$K_1^0(T) = 1.02 \times 10^{72}\ \text{atm}^{1/2}\ \text{cm}^3 \quad (27)$$

Finally, the activation energy E_u for electron hopping is 0.7 eV, based on the change in conductivity as a function of temperature at a fixed value of c for the lower temperatures at $Po_2 = 1.0$ atm where the $Fe^{\bullet}_{Al}$ concentration is controlled by background acceptors (Fig. 8). We have thus measured E_3 from the shift of the conductivity maximum as a function of Po_2 with temperature, and E_u from the temperature dependence of σ at a fixed Fe^{4+} concentration, i.e., fixed c. As shown in Eqs. (14)–(17), when at low Po_2, the background acceptors are balanced by oxygen vacancies, almost all of the iron ions are converted to $Fe^{3+}(c \approx 1)$. Equation (8) thus becomes

$$(1-c)^2\alpha Po_2^{1/2}\exp[(-(2E_3 - E_1)/kT)] \quad (28)$$

and the activation energy of the conductivity σ will be $(2E_3 - E_1 + 2E_u)/2$ where E_u is the hopping activation energy for holes in the 10%* Fe : YAG sample. Using the values of $E_1 = 7.8$ eV obtained from the Ce : YAG data, $E_3 = 1.9$ eV and $E_u = 0.7$ eV from the above analysis, we come up with an expected activation energy for conduction of 1.3 eV. In other words, the conductivity is predicted to decrease exponentially with increasing temperature. Indeed, the 1100°C isotherm begins to intercept the 1035°C isotherm under reducing conditions. Unfortunately, there is insufficient data at low Po_2 to see this trend more clearly.

Conduction via the iron Fe^{3+} band in garnets was previously observed by Larsen and Metselaar in YIG. The hopping activation energy of 0.7 eV is comparable to the value of 1 eV obtained for Fe^{4+} to Fe^{3+} hopping by Lal et al. [28–30] and Larsen and Metselaar [31]. Larsen and Metselaar [24] later reached a different conclusion for YIG in that the conduction is via a large polaron mechanism; however, since our data is for a narrower d band (with less than 10% iron), we do not necessarily disagree with this conclusion, namely that large polaron transport may occur in YIG, but small polaronic conductivity occurs in 10%* Fe : YAG in which the Fe bands are narrower.

6. Conclusion

We have measured the electrical properties of Fe : YAG. At low concentrations of Fe^{3+}, the iron does not effect the conductivity properties; rather background impurities determine the concentration of oxygen vacancies. The crystals are mixed conductors with ionic conductivity dominating at low Po_2 (with an activation energy of 2.6–2.8 eV) and a p-type conductivity at high-Po_2. High concentrations of iron induce an Fe band within the gap in which electronic carriers can conduct via a small polaron process with a hopping energy of 0.7 eV. The Fe band was found to lie 1.9 eV below the conduction band.

Acknowledgments

This research was supported in part by the MIT Center for Materials Science and Engineering under NSF Grant No. DMR-78-24185 and No. DMR-940034. The experimental part of the work was performed while the first author (S.R.R.) was at MIT. The authors wish to thank Donald Greer for assistance with fitting the data in Fig. 10.

References

1. G. Ziedler, *IEEE J. Quantum Electron.*, **QE-4**, 1016 (1968).
2. E.W. Duczynski, G. Huber, V.G. Ostroumov, and I.A. Shcherbakov, *Appl. Phys. Letts.*, **48**, 1562 (1986).

3. B.M. Antipenko, A.S. Glebov, T.I. Kiselva, and V.A. Pismennyi, *Opt. Spec*., **60**, 95 (1986).
4. J.M. Robertson, M.W. Van Tol, J.P.H. Heynen, and W.H. Smits, *Phil. J. Res*., **35**, 354 (1980).
5. D.P. Devor, L.G. DeShazaer, and R.C. Pastor, *IEEE J. Quantum Electron*., **QE-25**, 1863 (1989).
6. D.J. Robbins, B. Cockayne, J.C. Glasper, and B. Lent, *J. Electrochem. Soc*., **126**, 1213 (1979).
7. C.M. Wong, S.R. Rotman, and C. Warde, *Appl. Phys. Lett*., **44**, 1038 (1984).
8. S.R. Rotman, R.P. Tandon, and H.L. Tuller, *J. Appl. Phys*., **57**, 1951 (1985).
9. S.R. Rotman and C. Warde, *J. Appl. Phys*., **58**, 522 (1985).
10. S.R. Rotman and H.L. Tuller, *J. Appl. Phys*., **62**, 1305 (1987).
11. S.R. Rotman, M. Roth, H.L. Tuller, and C. Warde, *J. Appl. Phys*., **66**, 3207 (1989).
12. S.R. Rotman, H.L. Tuller, and C. Warde, *J. Appl. Phys*., **71**, 1209 (1992).
13. S.R. Rotman, C. Warde, H.L. Tuller, and J. Haggerty, *J. Appl. Phys*., **66**, 3207 (1989).
14. J.L. Bates and J.E. Garnier, *J. Am. Ceram. Soc*., **64**, C-138 (1981).
15. A.Y. Neiman, E.V. Tkachenko, and V.M. Zhukovskii, *Dokl. Akad. Nauk SSSR*, **240**, 876 (1978).
16. L. Schuh, R. Metselaar, and G. de With, *J. Appl. Phys*., **66**, 2627 (1989).
17. J.S. Haggerty, W.P. Menashi, and J.F. Wenkus, *Method for Forming Refractory Fibers by Laser Energy*, U.S. Patent No. 3,944,640, March 16, 1976.
18. J.S. Haggerty, W.P. Menashi, and J.F. Wenkus, *Apparatus for Forming Refractory Fibers*, U.S. Patent No. 4,012,213, March 15, 1977.
19. J.S. Haggerty and W.P. Menashi, *Production of Oxide Fibers by a Floating Zone Fiber Drawing Technique*, NASA, Contract No. NAS3-13479, February 1971.
20. R. Metselaar and P.K. Larsen, in *Physics of Magnetic Garnets*, edited by A. Paoletti (North- Holland, Amsterdam, 1978), pp. 417–444.
21. P.K. Larsen and R. Metselaar, *Mater. Res. Bull*., **8**, 883–92 (1973).
22. P.K. Larsen and R. Metselaar, *Phys. Rev. B*, **8**, 2016 (1973).
23. R. Metselaar and P.J. Larsen, *Solid. State Commun*., **15**, 291 (1974).
24. P.K. Larsen and R. Metselaar, *Phys. Rev. B*, **14**, 2520 (1976).
25. R. Kofstad, in *Nonstoichiometry, Diffusion and Electrical Conductivity in Binary Metal Oxides* (Wiley-Interscience, New York, NY, 1972). p. 99.
26. H. Fujimoto, *The Electrical Properties and Defect Structure of Doped Thorium Dioxide*, Ph.D. Thesis, Dept. of Materials Science and Engineering, Massachusetts Institute of Technology, Dec. 1981.
27. P. Kofstad, *Nonstoichiometry, Diffusion and Electrical Conductivity in Binary Metal Oxides* (Wiley-Interscience, New York, NY, 1972), p. 50.
28. V.R. Yadav and H.B. Lal, *Jpn. J. Appl. Phys*., **18**, 2229 (1979).
29. V.R. Yadav and H.B. Lal, *Canada J. Phys*., **57**, 1204 (1979).
30. H.B. Lal, B.K. Verma, and V.R. Yadav, *J. Mat. Sci*., **17**, 3317 (1982).
31. P.K. Larsen and R. Metselaar, *J. Sol. State Chem*., **123**, 253 (1975).